Design and Application of a Decoupled Rotary-Linear Switched Reluctance Motor for Concentrated Photovoltaic Power Generation

Siyang Li, K.W.E. Cheng*, Jingwei Zhu, Yu Zou

Department of Electrical Engineering, The Hong Kong Polytechnic University, Hong Kong
*eric-cheng.cheng@polyu.edu.hk

Abstract: A decoupled two-degree of freedom (2-DOF) switched reluctance motor is investigated for a special application in concentrated photovoltaic (CPV) power generation system. Firstly, a new method to adjust the gesture of solar cells by the motor is proposed. Second, the motor is introduced elaborately, including its structure, design and control. Importantly, this motor has been manufactured and initially used by the CPV power generation system. Thirdly, experimental measurements involving force outputs and torque outputs are given. The tracking accuracies in linear and rotary directions can achieve high accuracy in both degree of freedom of 0.3 degree and 100 um respectively that is utterly needed by CPV. As the results of the tracking upgraded, the power generation output of the new CPV system has been enhanced, validating the effectiveness of the motor and the solar tracking system proposed. This power generation approach can be used in solar energy harvesting in future.

1. Introduction

In seeking for high efficiency of PV generation systems, several methods are used to enhance the efficiency of solar cells, such as converters, control algorithms, maximum power-point tracking schemes [1-4]. Concentrated photovoltaic (CPV) power generation system, as a new type of solar energy harvesting method, has been investigated for several years. One of popular solar cells for CPV power generation system is a triple-junction made of GaInP (1.9 eV), GaAs (1.4 eV), Ge (0.7 eV). The recorded efficiency has achieved 41% under concentrated sunlight AM1.5D illumination. As we know, a conventional optical part of the concentrator is composed of parabolic dish focusing reflector and Fresnel focusing lens. Fresnel focusing lens is popular in CPV power generation systems in recent years, because, compared with the other lens, it can reduce some expensive materials and improve the conversion efficiency. Researchers focus the solar power generation on CPV power generations because of the improved efficiency by a precise solar tracker. Therefore, the solar tracking system is the core part in CPV power generation system to reach the maximum power output for the power generation system. Generally, to keep the tracking error less than 0.5 ° is utterly needed for CPV; a solar sensor is employed to feedback the angle of the solar cell and sunlight in real time. It is necessary to adjust the CPV very accurately in order for, the solar cells reach the plane vertical to sunlight [5-7]. The solar tracking system usually consists two axes of rotation of azimuth and inclination with accurate tracking devices in order to increase the power conversion efficiency. As shown in the Fig 1 (a), the traditional CPV modules can rotate from 0 ° to 180 ° vertically and 90 ° to 180 ° horizontally with two gears.

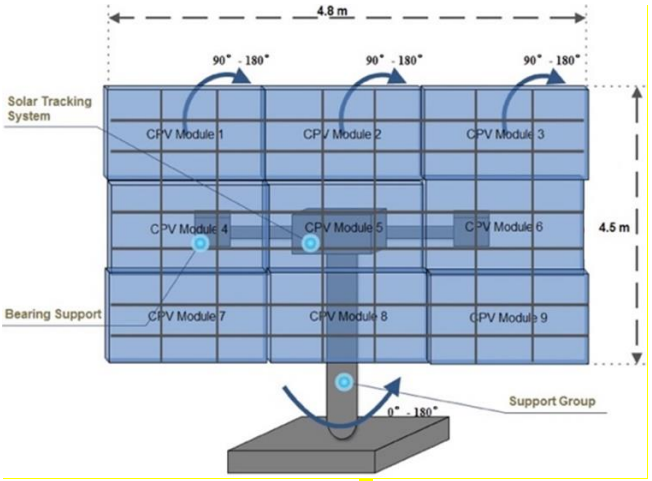

a

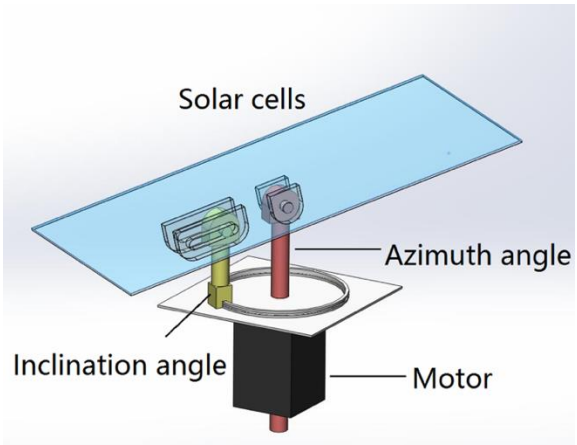

b

Fig. 1.
(a) *The overall mechanical structure of CPV system* ***(b)*** *The mechanical configuration for solar tracking system structure*

Traditional solar tracking systems are two directions of azimuth and inclination of cogwheels, which are driven by two motors with drive pinions. It utilizes a steel structure to fasten the CPV modules with large size and weight. In Fig.1 (b), the new tracking system is only based on a two-degree rotary-linear motor to complete all tracking operations. A two-degree motor has combined the CPV modules and support group together. The inclination angle tracking is achieved by the linear motion of the motor and the azimuth angle tracking is achieved by the rotating motion of the motor. The comparison of the proposed simple tracking system with the traditional one show that, not only the size and weight of new tracker is reduced, but also the tracking precision can be improved.

Traditional mechanical tracking systems usually take advantage of electrical machines as the executors, including direct current (DC) motors, such as permanent magnet (PM) brushless direct current motors (BLDCM) and alternating current (AC) motors to control the gesture of the solar panel [8]. However, conventional approaches cannot avoid some drawbacks. The deteriorated working environment, such as high temperature and vibration, could cause demagnetization to the permanent magnets. Hydraulic motors and gear motors are also used to control the position of the panel, which needs to be maintained periodically [9]. According to the weight and volume of CPV module, the mechanical devices have been considered, such as transmission gear boxes, connecting rods etc. which are traditionally applied to change the speed and torque of the motor simultaneously [10]. If there are over two actuators to realize the gesture regulation, it will not only increase the number of mechanical subsystem and the entire cost of the system, but also reduce the position tracking accuracy. Meanwhile, the growing number of intermediate mechanical converters will increase more maintenance for the system [11-12].

To tackle the problems mentioned above, the concept of two-dimensional should be used. Although such motor exists but their accuracy in angle control is not satisfactory. A new application of rotary-linear machine based on switched reluctance motor is put forward for the industrial motion control equipment [13-14]. Rotary-linear switched reluctance motors (RLSRMs) are usually implemented in industry applications, such as boring mill, drill press and carving machines, etc. Conventional machines are described in [15] and [16], and such motions are commonly realized by two independent motors and some mechanical connection parts. However, the traditional designs cannot avoid the drawbacks of complex mechanical structures and control methods, thus reducing their tracking accuracy. Nowadays, the direct-drive machine has the advantages of a high tracking accuracy and simplified mechanical configuration indicating its wide range application.

In [17-19], the principles of the actuator based on the permanent magnet synchronous motor (PMSM) are discussed. However, it is not suitable for the simultaneous movements of rotating and linear pulsing, because of its complex control method and operating environment restriction. There are other configurations focused on induction motors [20], and stepper motors [21]. Unfortunately, neither of them is applied to widespread occasions. Therefore, the switched reluctance (SR) machines are suitable to be used in industry, due to the advantages of the mechanical stability and simple structure. Moreover, an RLSRM was presented to integrate rotating and linear motion [22-25]. In [22] and [24], the coupling effect has occurred when both the rotary and linear motions are produced by the same coils. Although the coupling effect is eliminated in [23], the volume of the whole motor is quite large and linear motion will affect the torque output of the rotatory part greatly when linear move and rotation are operated simultaneously. In [25], different windings are utilized for rotary and linear motion, however, the linear motion still has a negative effect on the rotary motion and the whole volume is large. Therefore, the decoupled control methods have been investigated in [26-29], where reasonable distribution control of the current is achieved, and the decoupling action of both rotation and linear motion is implemented. Therefore, the control accuracy has been improved. Since the switched reluctance motor is selected as the actuator, not only the efficiency of it is lower than other kinds of motors, but also the force volume ratio is relatively small. Although the rotating linear motor has been controlled by the method of the decoupling, it cannot solve the problems of the lower conversion efficiency, the smaller torque and linear direction force.

In this paper, a new RLSRM is investigated in this paper. Its property of physically decoupled structure has been highly investigated, and the tracking precision increases by using a simple control scheme. Moreover, the concept is confirmed by finite element method (FEM). The experimental results prove that the errors of rotary and linear tracking can be controlled within 0.3° and 100 μm, respectively. On the basis of the high tracking precision and conversion efficiency, the improvement of output power has been verified.

2. Construction of the motor

The RLSRM combines a 4-phase LSRM and a 3-phase RSRM together using longitudinal fluxes and transvers fluxes, as shown in Fig.2 (a). The basic specifications are exhibited in Table I. The outside part controls the moving shaft for linear motion, while the inside part, which is an inner stator and outer rotor structure, dominates the rotary motion. The core of the machine is that the rotor is screwed on the shaft and the moving part can achieve a linear-rotary motion. The shaft is supported by two bearings. The moving part has been fully embraced by solid aluminium. The linear stator relates to and fixed on the outside stator base of the RLSRM. Fig.2 (b) is the side views of the proposed motor.

According to the structure in Fig. 2 (a), the moving part is completely physically decoupled for the linear and rotary movements. Therefore, the difficulty of manufacturing has been reduced significantly. Moreover, the linear and rotary movements can be controlled individually, and there is no electromagnetic interference between them. Meanwhile, by optimizing and simplifying the control method, high-precision tracking can be realized as well. Fig.2 (c) shows the prototype of the proposed motor. The advantages of the motor topology can be summarized as follows:

1) Any decoupling control method is not needed; there are no interferences between the rotary part and linear part;

2) Control method is simpler and easier, and the movements of rotary and linear can be controlled independently;

3) Force of linear motion is increased with high tracking precision.

4) Robust mechanical configuration is achieved for RLSRMs.

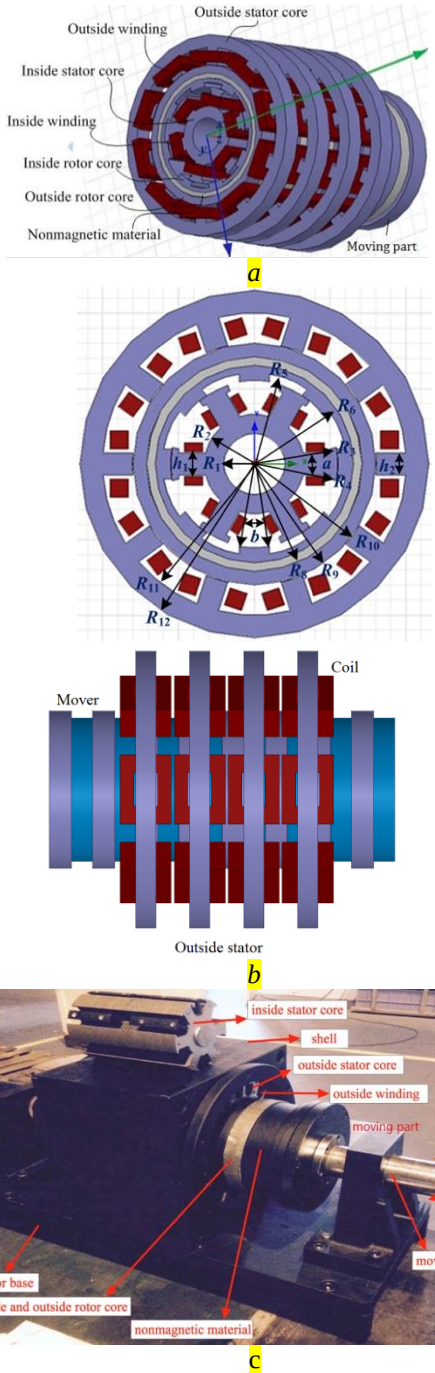

Fig.2. (a) *Configuration of the proposed motor.* ***(b)*** *side views of the proposed motor and* ***(c)*** *prototype of the motor*

Table 1 The main specifications of the motor

Symbol	Specification	Value
R_1	Inside stator radius	20 mm
R_2	Inside stator radius	33 mm
R_3	Inside stator radius	55 mm
R_4	Inside rotor radius	55.4 mm
R_5	Inside rotor radius	60.4 mm
R_6	Inside rotor radius	65.4 mm
R_8	Outside rotor radius	71 mm
R_9	Outside rotor radius	80 mm
R_{10}	Outside stator radius	80.3 mm
R_{11}	Outside stator radius	100 mm
R_{12}	Outside stator radius	115 mm
h_1	Inside stator yoke	15 mm
h_2	Outside stator yoke	15 mm
a	Inside stator angle	23 ˚
b	Outside stator angle	21 ˚
M	Mass of the moving platform	25 kg
g_a	Inside air gap length	0.3 mm
g_b	Outside air gap length	0.5 mm
q_1	Number of phases	3
q_2	Number of phases	4
N_{ph1}	Turn number of inside winding	106
N_{ph2}	Turn number of outside winding	70

3. Theoretical analysis

3.1. The linear section

The exact specifications of the linear section include the maximum velocity of 1.0 m/s, and the acceleration time of 0.167 s. So, the acceleration can be defined by:

$$a = 5.98 \text{ m/s}^2 \quad (1)$$

The maximum mass for the moving part is 25 kg. Then, average thrust force can be calculated as:

$$F = M \cdot a = 149.5 \text{ N} \quad (2)$$

The power capacity is given by:

$$P = F \cdot v = 149.5 \text{ W} \quad (3)$$

3.2. The rotary section

Assume that q is the number of phases. e_a and i_a are the induced electromotive force and current in each phase winding, respectively. K_d is load factor of each phase in a switching period. Then, the electromagnetic power is calculated as:

$$P_{em} = q \cdot e_a \cdot i_a \cdot K_d = 400 \text{ W} \quad (4)$$

D_a is the diameter of rotor, and N_r is the number of the rotor poles. The rotor pole pitch is:

$$\tau_r = \pi \cdot \frac{D_a}{N_r} \quad (5)$$

Φ is the main flux with each $\theta_{off,}$ and l_δ is the length of the stator base. Therefore, the magnetic load is defined by:

$$B_\delta = \frac{\phi}{\tau_r \cdot l_\delta} \tag{6}$$

The electromagnetic torque is given by:

$$T_{em} = \frac{P_{em}}{\omega} = 16.71 \text{ N} \cdot \text{m} \tag{7}$$

According to the winding current I, and the number of turns per phase N_{ph}. The electrical load can be calculated as:

$$A = \frac{q \cdot N_{ph} \cdot I}{\pi \cdot D_{si}} \tag{8}$$

Based on the cross-sectional area of conductor S_a, the electric current density is calculated:

$$J = \frac{I}{S_a} = \frac{(\pi \cdot D_a \cdot A)/(q \cdot N_{ph})}{S_a} = 5.006 \text{ A/mm}^2 \tag{9}$$

4. Performance and simulation results

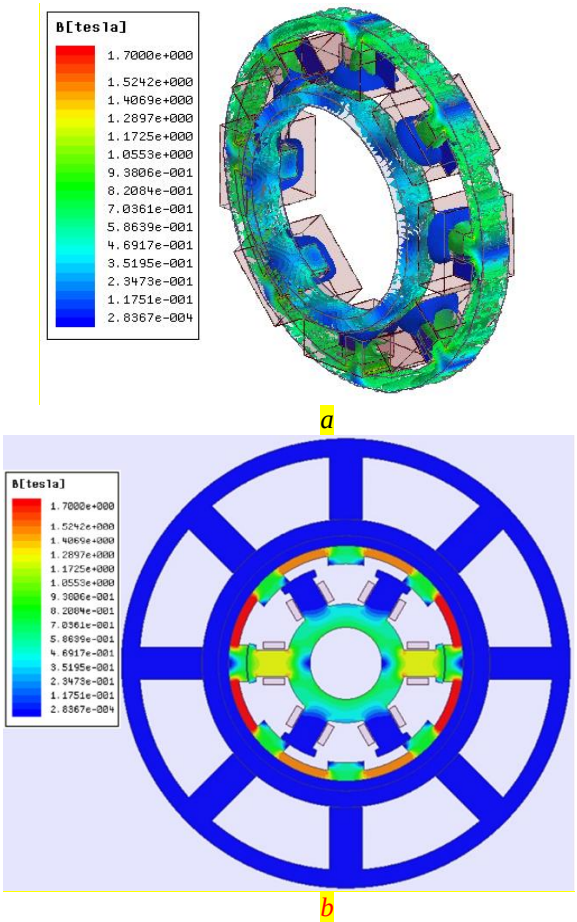

Fig.3. (a) *Magnetic field distribution of linear section and* ***(b)*** *Magnetic field distribution of rotary section*

To analyse the magnetic field distribution and properties of the motor, FEM calculation is utilized. Fig.3 (a) is the magnetic field distribution of the linear section by using 3-D FEM when the excitation current is 2 A. And Fig.3 (b) is the magnetic field distribution of rotary section by using 2-D FEM under the rated current 10 A. It can be seen that the decoupled property has been achieved completely.

Fig.4 (a) and (b) shows the waveforms of the linear force and the rotary torque by using FEM calculation. Both of the two sections are given based on the corresponding phase current levels with different colors. The simulation result shows that the linear force achieves over 150 N under the rated current 10 Ampere. For rotary section, the torque of ±7.2 N·m is realized. Furthermore, the inductance property of the linear stator is shown in Fig.4 (c).

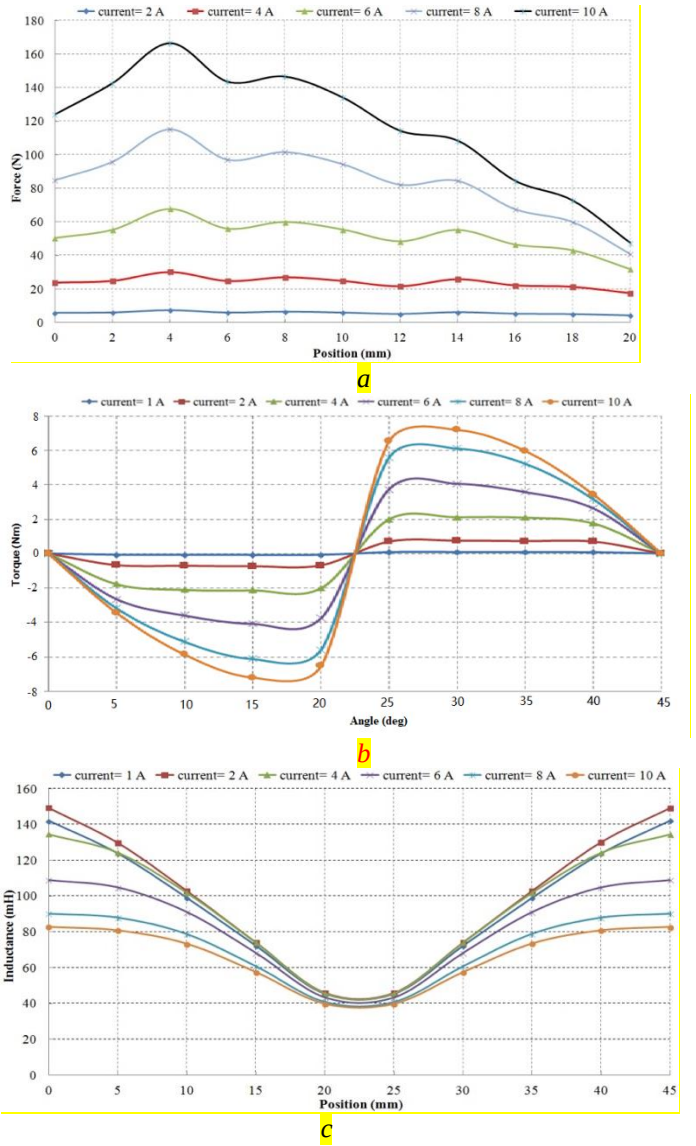

Fig.4.(a)*waveforms of FEM calculation of linear section,* ***(b)*** *waveforms of FEM calculation of rotary section, and* ***(c)****Inductance performance of the linear part*

5. Page Formatting Performance and simulation results

5.1. The configuration of controller

The controller of the solar tracking system consists of a single chip microcomputer (MCU), a solar sensor, a GPS module, a wind sensor and a motor drive system. The controller mainly obtains the position signal of the sun with the help of the solar sensor, and converts it into the angle signal through mathematical calculation. Then, the MCU sends the angle signal to the motor drive system, and the proposed motor is started for tracking. The diagram of the

controller configuration is shown in Fig.5 (a), and (b) is the flow chart of the essential operation of solar tracking system.

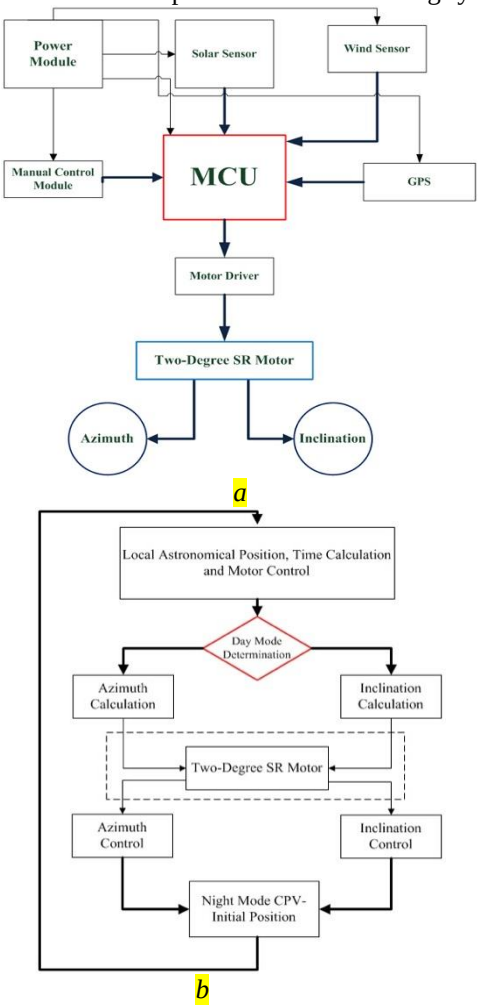

Fig.5. (a) *the diagram of the configuration of the controller,* ***(b)*** *the flow chart of the essential operation of the solar tracking system*

5.2. The control method

The control method can be roughly divided into two broad categories. One is open-loop control, for which the sun's trajectory parameters are required to be programmed into the equipment in the form of geographic coordinates beforehand, and then the system will track automatically based on the values in the coordinates. The other one is closed-loop control, which depends on the angle signals feedback by the solar sensor attached at the side of the CPV modules. The responsibility of the solar sensor is to measure the position of the sun and send the signal back to the tracking controller, and eventually the angle error between the real direction of the sunlight and that of the normal vector of the CPV modules will be corrected by two motors.

θ_z is represented by the inclination angle in the mathematic model and it can be calculated as follows [28]:

$$\sin\theta_z = \sin\phi \cdot \sin\delta + \cos\phi \cdot \cos\delta \cdot \cos\omega \quad (10)$$

where:

θ_z : The altitude angle in the system (θ_z = 90 º - sun's zenith angle)

Ø : The latitude ϕ= 22 º is the location

ω: The hour angle (15 º /hour)

δ : The solar declination

$$\delta = 23.45° \cdot \sin\left[\frac{360}{365}(284 + N)\right] \quad (11)$$

In this equation, *N* is the ordinal number of the day in the whole year (from 1 to 365). The relationship between the Azimuth angle and the inclination angle can be obtained from this equation:

$$\sin\theta_A = \frac{\cos\delta \cdot \sin\omega}{\cos\theta_z} \quad (12)$$

5.3. The position control scheme

The control system is responsible for linear and rotary motion separately. The feedbacks of both the two movements of angle and position are sampled by their own position sensors. Controllers output the force and torque reference commands for the force to current part and torque to current distribution part, respectively. Finally, the two-distribution parts output current commands for the drivers to control the motor. The closed current control based on proportional–integral algorithm with pulse width modulation (PWM) is performed inside the current drivers for precise current control. The trajectories of the two axes for the motor are shown below in Fig.6.

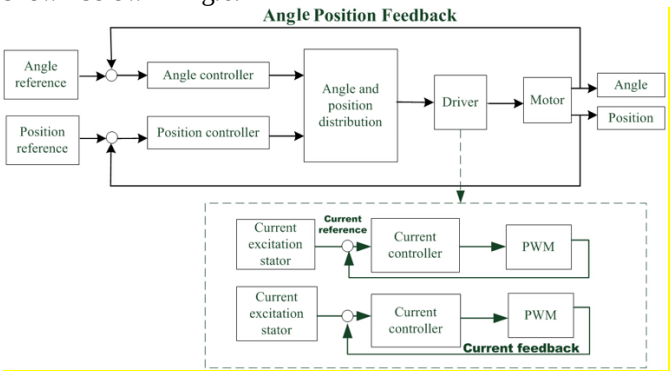

Fig.6. *Control block for the proposed machine*

It can be seen that the proposed motor is able to govern the movement of the power generation system. The simple PID controller can be applied in angular and linear position control with the control parameters in Table II.

Table 2 Parameters of the controller

Parameters	Angular position	Linear position
P	0.410	32.5
I	6.066	2.20
D	0.005	0.008

6. Experimental results

6.1. Force and Torque outputs

The force and torque outputs of the motor has been measured, as shown in Fig.7 (a) is the measured force outputs under different currents at 6 A, 8 A and 10 A, respectively, and (b) is the torque outputs as well.

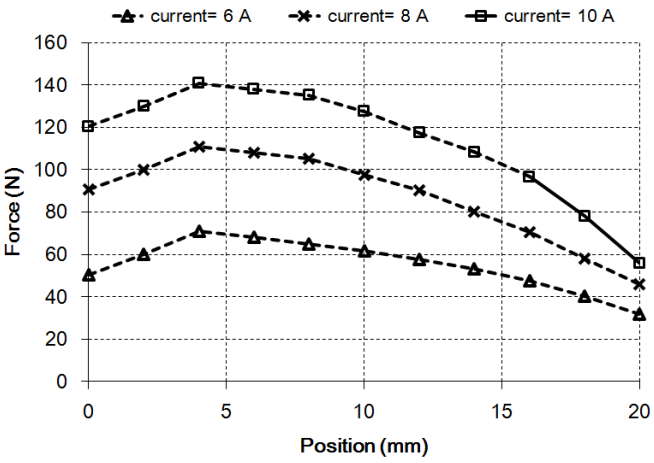

a

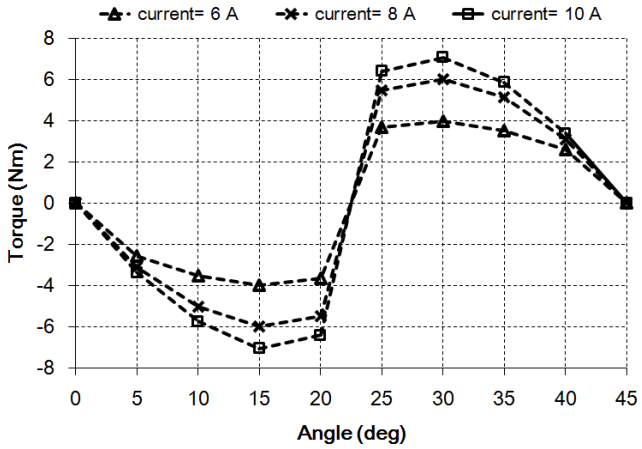

b

Fig.7. (a) *Force outputs measurement,* ***(b)*** *Torque outputs*

Fig. 8 shows the pictures of the proposed CPV power generation system. The tracking position of the motor is obtained by experimental tests. The whole experimental set up consists of a computer, a dSPACE DS1104 card, a power supplier, a driver and the motor, as shown in Fig.10. The control scheme as well as the controllers is built using the software package MATLAB/Simulink. The entire Simulink software will be programmed and debugged into the dSPACE card which is regarded as a hardware controller. This control card outputs commands to the driver for the motor after getting the position and rotational feedbacks from two encoders fixed on the motor's shaft, constructing a closed loop control. The position information for linear and rotary movement through experiments in laboratory can be obtained from Fig. 9 (a) and (b). The results indicate that the position tracking for rotation and linear motions without any decoupling method is capable of regulating the two axes.

a *b*

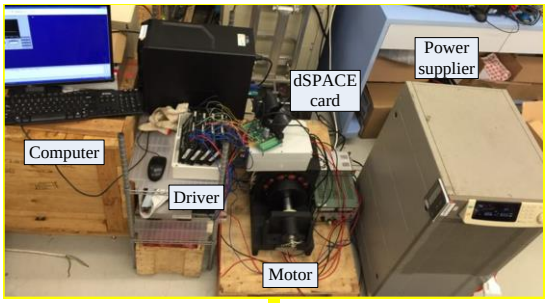

c

d

Fig.8.*Constructed RLSRM****(a)*** *Mover structure.* ***(b)*** *Outside winding.* ***(c)*** *experimental measurement for position control and* ***(d)****The prototype of CPV solar tracking system*

The dynamic tracking error response is shown in Fig. 9 (c) and (d). The control system is able to track position command signals precisely with slight vibration errors within 0.3 ° and 100 μm for the rotary and linear axes, respectively. Therefore, the tracking precision can ensure within 0.3 °. The tacking position accuracy will be improved and energy conversion efficiency for the system would be enhanced.

However, the vibration of waveform shows that the motor also vibrated during the process. Obviously, this vibration is a factor of efficiency loss of motor. In order to eliminate the influence, the aluminium plate attached to the stator should be thickened. Therefore, not only the efficiency will be improved, but also the tracking precision will be higher.

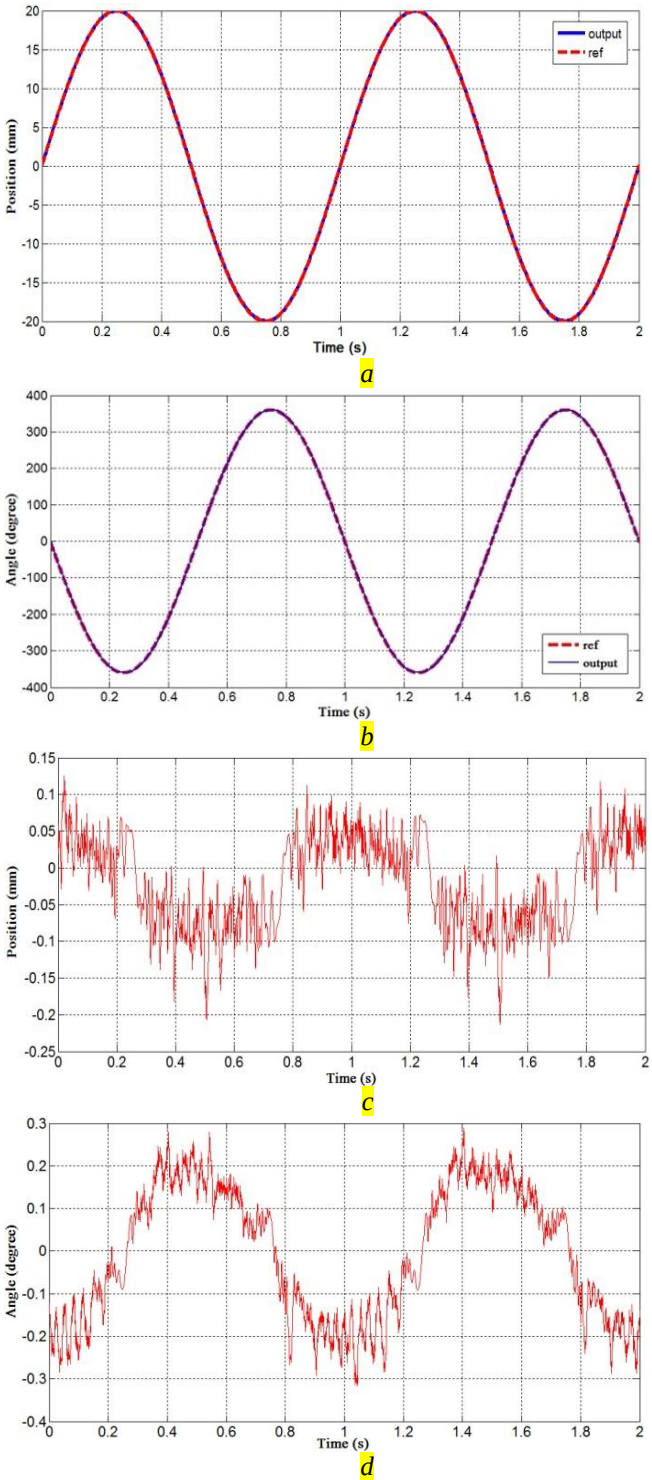

Fig.9. *Rotary-linear responses* ***(a)*** *and* ***(b)****, and their errors* ***(c)*** *and* ***d (d)***

6.2. Power outputs of the solar system

In order to verify the improvement of the output power with the proposed solar tracker, the power output of the system has been tested. Based on the CPV power generation system for the experiment B, its detailed specifications and parameters are shown in Table III.

Table 3 Main specification of the power generation system

Parameters	Value	Notes
I_{sc}	6.91 A	Short circuit current
B_{in}	90 W	Max power output (per module)
V_{oc}	18.6 V	Open circuit voltage
T_{emp}	25˚C	Temperature
I_{rr}	850 W/m^2	Power output per square meter
Weight	1300kg	(Maximum load)
Tracking precision	0.5°	Accuracy requirements

Fig.10 (a) and (b) are the measured results of the output voltage, current and output power of a CPV module (90 W) against different loads under 15 MJ/m^2 on 8th, November 2016, respectively.

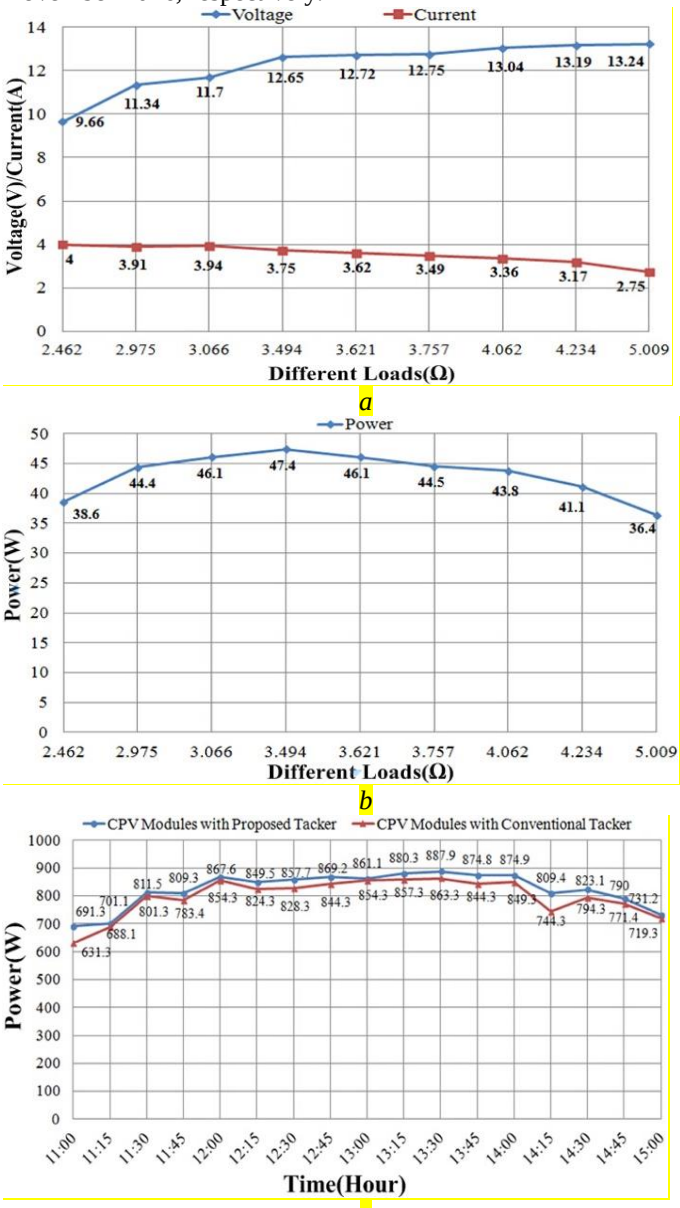

Fig.10. ***(a)*** *Measured results of the output voltage and current versus different loads.* ***(b)*** *Measured results of the output power versus different loads, and* ***(c)*** *Measured results of the output power with two different solar trackers on 8th, November 2016*

It was found that with the load increasing, the output voltage goes up while the value of the current decreases. The output power reaches its highest value, approaching 47.4 W when the load is 3.494 Ω. When the load increases from 3.494 Ω to 5.009 Ω, the output power will decline rapidly.

Fig.10 (c) shows the comparison of the measured output power between the proposed solar tracker and conventional solar tracker on 8th, November 2016. The output power was improved by using the proposed solar tracker with the two-degree freedom rotary-linear SR motor. The efficiency was enhanced by 2.78 % at the maximum power point at 13:30. Consequently, the improvement of conversion efficiency and output power of proposed solar tracking system was achieved.

7. Conclusion

In this paper, a new RLSRM is proposed, and the major design parameters are calculated, including both of linear and rotary sections. The results of FEM confirm the feasibility of the RLSRM decoupled design. Also, the experimental test result shows that decoupling is achieved when the linear motion and rotation are operated simultaneously. Finally, PID control scheme is put forward for the motor to achieve a decoupled high position tracking accuracy in CPV. The tracking errors are 0.3 ° and 100 μm for the rotary and linear axes, respectively. With the same current, not only the linear force achieved 150 N, but also the torque is ±7.2 N·m.

The proposed motor has been applied to the solar tracking system for CPV power generation system to track the sun accurately. Its theoretical analysis, configuration and control method are described in detail. The achievements of experiment have verified the improvements output power, which is enhanced by 2.78 %, respectively. It is a successful development for real application in CPV. Apart from this application, it is expected that this motor can be used by two-dimensional drilling or welding equipment.

8. References

[1] Bader N. Alajmi, Khaled H. Ahmed, tephen J. Finney; Barry W. Williams, 'A Maximum Power Point Tracking Technique for Partially Shaded Photovoltaic Systems in Micro grids,' *IEEE Trans. Ind. Electron*, 2013, 60, (4), pp. 1596-1606.

[2] Pandey, A., Nitya Power Technol. Pvt., Ltd., Delhi, Dasgupta, N., Mukerjee, A.K., 'High-Performance Algorithms for Drift Avoidance and Fast Tracking in Solar MPPT System', *IEEE Trans. Energy Convers*, 2008, 23, (2), pp. 681-689.

[3] Seyedmahmoudian, M.,Horan, B., Rahmani, R., Oo, A.M.T., Stojcevski, ' A. Efficient photovoltaic system maximum power point tracking using a new technique,' *Energies* , 2016, 9, (147), pp.147.

[4] Fu-Sheng Pai, Ru-Min Chao, Shin Hong Ko, Tai-Sheng Lee., 'Performance Evaluation of Parabolic Prediction to Maximum Power Point Tracking for PV Array,' *IEEE Trans. Sustainable Energy*, 2008, 2, (1), pp. 60-68.

[5] Xiaoli Xu, Qiushuang Liu, YunboZuo, 'A Study on All-Weather Flexible Auto-Tracking Control Strategy of High-Efficiency Solar Concentrating Photovoltaic Power Generation System,' *Second WRI Global Congress on Intelligent Systems (GCIS), Feb 2011.*

[6]Cong-Hui Huang, Heng-Yau Pan, Kuan-Chan Lin, 'Development of Intelligent Fuzzy Controller for a Two-Axis Solar Tracking System,' *Appl.Sci*, 2016, 6, (130).

[7] Alberto Dolara, Francesco Grimaccia, Sonia Leva, Marco Mussetta, Roberto Faranda, MorisGualdoni., 'Performance Analysis of a Single-Axis Tracking PV System,' *IEEE Journal of Photovoltaics*. 2012, 2, (4), pp. 524-531.

[8] Juncai Song, Fei Dong; Jiwen Zhao, Siliang Lu; Le Li, Zhenbao Pan, 'A New Design Optimization Method for Permanent Magnet Synchronous Linear Motors,' *Energies*, 2016, 9(12), pp.992.

[9] Ping Zheng, Chengde Tong, Jingang Bai, Jing Zhao, Yi Sui, Zhiyi Song, 'Modelling and Control of a Flux-Modulated Compound-Structure Permanent-Magnet Synchronous Machine for Hybrid Electric Vehicles,' *Energies*, vol. 2012, 5, (1), pp. 45-57.

[10] Menoufi K, Chemisana D, Rosell, J.I, 'Life Cycle Assessment of a Building Integrated Concentrated Photovoltaic scheme', *Appl. Energy*, 2013, 111, pp. 505–514.

[11] Jain, S., Agarwal, V.: 'Comparison of the performance of maximum power point tracking schemes applied to single-stage grid-connected photovoltaic systems', *IET Electr. Power Appl.*, 2007, 1, (5), pp. 753–762.

[12] E. Suresh Kumar, Bijan Sarkar, 'Impact of Wind and Shading on Energy Contribution by Photovoltaic Panels with Axis Tracking System,' International Conference on Microelectronics, *Communication and Renewable Energy*, Aug 2013.

[13] R. Cao, M. Cheng, C. Mi, W. Hua, and W. Zhao, 'Comparison of complementary and modular linear flux-switching motors with different mover and stator pole pitch,' *IEEE Trans. Magn.*, 2013, 49, (4), pp. 1493–1504.

[14] X. D. Xue, K. W. E. Cheng and S. L. Ho, "A Self-Training Numerical Method to Calculate the Magnetic Characteristics for Switched Reluctance Motor Drives", IEEE Trans on Magnetics, Vol. 40, Issue: 2 , March 2004, Pp734 – 737.

[15]C. T. Liu and T. S. Chiang, 'Design and performance evaluation of a micro linear switched-reluctance motor,' *IEEE Trans. Magn.*, 2004, 40, (2), pp. 806–809.

[16] G. Baoming, A. T. de Almeida, and F. Ferreira, 'Design of transverse flux linear switched reluctance motor,' *IEEE Trans. Magn.*, 2009, 45, pp. 113-119.

[17] K. J. Meessen, J. J. H. Paulides, and E. A. Lomonova, 'Analysis of a novel magnetization pattern for 2-DoF rotary-

linear actuators,' *IEEE Trans. Magn.*, 2012, 48(11), 3867-3870.

[18] T. T. Overboom, J. W. Jansen, E. A. Lomonova, and F. J. F. Tacken,'Design and optimization of a rotary actuator for a two-degreeof freedom zϕ-module,'*IEEE Trans. Ind. Appl*., 2010, 46, (6), pp. 2401–2409.

[19] G. Krebs, A. Tounzi, B. Pauwels, D. Willemot, and F. Piriou, 'Modeling of a linear and rotary permanent magnet actuator,'*IEEE Trans. Magn*., 2008,44, (11), pp. 4357–4360.

[20] J. H. H. Alwash, A. D. Mohssen, and A. S. Abdi, "Helical motion tubular induction motor," *IEEE Trans. Energy Convers*., 2003, 18, (3), pp. 362–369.

[21] Y. H. Kim, C. S. Jin, S. Kim, Y. D. Chun, and J. Lee, 'Analysis of hybrid stepping motor using 3D equivalent magnetic circuit network method based on trapezoidal element,'*J. Appl. Phys.*, 2002, 91, (10), pp. 8311–8313.

[22] Y. Sato, 'Development of a 2-degree-of freedom rotational / linear switched reluctance motor,'*IEEE Trans. Magn*., 2007, 43, (6), pp. 2564-2566.

[23] Mohammad Mehdi Nezamabadi, Ebrahim Afjei, and Hossein Torkaman,'Design, Dynamic Electromagnetic Analysis, FEM, and Fabrication of a New Switched-Reluctance Motor with Hybrid Motion,' *IEEE Trans. Magn.*, 2016, 52, (4).

[24] L. Szabó, I. Benţia, M. Ruba, 'A rotary-linear switched reluctance motor for automotive applications,' in *Proceedings of the 20th International Conference on Electrical Machines (ICEM) Marseille (France)*, pp. 2615-2621, 2012.

[25] J. Pan, N. Cheung, G. Cao, 'Investigation of a rotary-linear switched reluctance motor,' in Proceedings of the *XIX International Conference on Electrical Machines (ICEM)*, Rome (Italy), 2010, pp. 1-4, 2010.

[26] Pan, Yu Zou, Cheng. N. C, 'Performance analysis and decoupling control of an integrated rotary–linear E. R. Pelta: "Two-axis Sawyer motor for motion systems,' *IEEE Control Systems Mag*., 1987, pp. 0-24.

[27] Liu C T and Kuo J L, 'Experimental investigation and 3-D modelling of linear variable reluctance machine with magnetic-flux decoupled windings,' *IEEE Trans. Magn.*, 1994, 30, pp. 4737–4739.

[28] J.K.Lin, K.W.E.Cheng, "Active Suspension System Based on Linear Switched Reluctance Actuator and Control Schemes", IEEE Transactions on Vehicular Technology, Vol. 62, Issue: 2, 2013, pp. 562 – 572.

[29] Pan, J.F., Fanjie, Meng., Guangzhong, C., 'Decoupled control for integrated rotary-linear switched reluctance motor,' *IET Electr. Power Appl*., 2014, 8, (5), pp. 199–208.